Final Draft

of the original manuscript

Gießgen, T.; Mittelbach, A.; Höche, D.; Zheludkevich, M.; Kainer, K.:

Enhanced predictive corrosion modeling with implicit corrosion products.

In: Materials and Corrosion. Vol. 70 (2019) 12, 2247 - 2255.

First published online by Wiley: 22.08.2019

https://dx.doi.org/10.1002/maco.201911101

Enhanced predictive corrosion modeling with implicit corrosion products

Tom Gießgen[1] **Andreas Mittelbach**[1] **Daniel Höche**[2,3]

Mikhail Zheludkevich[2] **Karl U. Kainer**[2]

[1]Daimler AG, Entwicklung
Mercedes-Benz Cars, Sindelfingen, Germany
[2]Helmholtz-Zentrum Geesthacht, Institute for Materials Research, Corrosion and Surface Technology, Geesthacht, Germany
[3]Faculty of Mechanical Engineering, Computational Material Design,
Helmut-Schmidt-University, Hamburg, Germany

Correspondence
Andreas Mittelbach, Daimler AG, Entwicklung Mercedes-Benz Cars, HPC X316, DE-71059 Sindelfingen, Germany. Email: andreas.mittelbach@daimler.com

Abstract

An advanced mathematical approach to describe the influence of corrosion products on the corrosion rate is presented here. The related model can be used as input equation for numerical predictive corrosion simulations or simply as an empirical model, to extrapolate experimental data of corrosion tests to longer times and to interpret the physical parameters behind. This semiempirical model assumes that a constant share of the dissolved metal precipitates on the surface and hinders the diffusion processes. Hence, the effective corrosion rate decreases exponentially with increasing dissolution. The explicit corrosion progress over time is derived by time integration on a newly developed, time dependent corrosion rate equation. The derived expression can be effortlessly implemented in existing for example finite element method, which is demonstrated for the uniform corrosion of a zinc surface. Furthermore, this approach is qualitatively compared with other empirical models for corrosion products and the validity is demonstrated by fitting of experimental data. A very good agreement between experiment and theory can be achieved for various materials and environments considering no change of the driving corrosion mechanism.

1 INTRODUCTION

Modeling of corrosion processes is a research subject of great interest and has applications among others in automotive industry,[1–3] marine industry,[4–6] and medical industry.[7,8] There are various approaches to compute the corrosion progress. One approach suitable for long time and length scales, for example corrosion of ship hulls, is empirical modeling since it is not computational expensive and can be considered as valid until changes of the corrosion driving mechanism can be excluded. The qualitative corrosion progress is proposed in these models and the parameters are found by fitting the experimental data. There are different qualitative descriptions how much the corrosion products retard the dissolution of the metal surface.[4,5,9] On short time and length scales, microscopic models (incl. electronic and atomistic models) are often employed to compute the initiation stage, and the reaction rates and migration processes of the participating chemical species.[6,10–12] While this approach allows to accurately model the creation and the influence of corrosion products, it is computationally expensive. Simulation times over decades can be achieved, if the deformation of the metal

surface due to the anodic dissolution is neglected or relatively small compared to the whole geometry size.[13]

The so-called mixed potential theory (MPT) for electrochemical systems allows to model corrosion processes including the surface deformation on larger time and length scales if the system can be described correctly by anodic and cathodic reactions and electric field equations. For example, metal sheets with widths of several millimeters can be simulated over the timespan of weeks or months just considering the near surface electrochemistry respectively electric field.[1–3,14,15] However, the authors are not aware of a MPT study describing the effects of corrosion products without computing the ion concentrations, despite its high demand in corrosion engineering.

This article presents a new implicit model for corrosion products, which modifies the effective corrosion rate depending on the amount of dissolved metal and respective formed corrosion products. It can be implemented in any continuum approach like finite element method (FEM) simulations and allows efficient implementation of corrosion products into nonionic mathematical corrosion modeling approaches. By integrating the corrosion rate, the analytic expression of the corrosion progress is obtained, which might be useful as an empirical model to extrapolate experimental data and to predict critical corrosion induced failure more accurate. The proposed model assumes a kinetic control of the corrosion rate like on bare metal surfaces, which continuously turns into diffusion control process linked to the precipitation of corrosion products similar to the so-called bi-modal model by Melchers.[16]

2 | COMPUTATIONAL MODELING

2.1 | Governing equations

The current FEM based model originates from for galvanic corrosion model presented by Deshpande[1] and Höche[6] with modifications from Shaik and Thamida[17] and Gießgen et al.[15] to account for uniform corrosion. Following assumptions and simplifications are made:

1. Homogeneous electrolyte with constant conductivity ($\sigma = 7{,}95\,\mathrm{S/m}$[3])
2. Electro-neutrality
3. Incompressibility

This model is also often referred to and named as the MPT based approach.[1–3,6,14,15] The Nernst–Plank equation, which physio-chemically describes this system, reduces with these assumptions to

$$\Delta\phi = 0. \tag{1}$$

ϕ is the electrolyte potential with following boundary conditions

$$\nabla_{\mathrm{n}}\phi = \begin{cases} 0, & \text{insulating boundary} \\ i(\phi)/\sigma, & \text{electrodes.} \end{cases} \tag{2}$$

$i(\phi)$ is the electric current according to the respective polarization curve of the electrode's material without corrosion products. The electric potential ϕ_{M} within the metal is computed accordingly. The conductivity of zinc is $\sigma_{\mathrm{Zn}} = 1.7\mathrm{E}7\,\mathrm{S/m}$.[18] The relevant equations and the simple simulation geometry are visualized in Figure 1.

The corrosion progress y within a time interval Δt at the right-hand site of the figure due to the anodic current density i_{a} is computed applying Faraday's law[19]

$$y = \frac{i_{\mathrm{a}}\,\Delta t M}{z\rho F}. \tag{3}$$

M denotes the molar mass, z the electron number, ρ the density of the metal, and $F = 9{,}649\mathrm{E}4\,\mathrm{C/mol}$ is the Faraday constant. Based on this simple model an adaption to uniform corrosion is possible as shown in the following.

2.2 | Modeling uniform corrosion

This section briefly describes the modification of the MPT to model corrosion of a uniform metal surface from a previous publication by the current authors.[15] The homogenous metal surface is divided into multiple microelectrodes as proposed by Shaik and Thamida.[17] The boundary condition for each microelectrode is chosen randomly from two possible polarization curves with probability 0.5. One of both curves was measured in an oxygen-rich electrolyte to characterize the cathodic oxygen reduction. The second polarization curve was

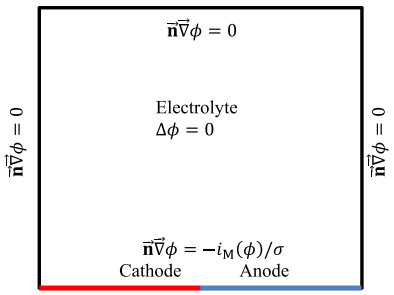

FIGURE 1 Scheme of the corrosion simulation via the mixed potential theory adapted from Deshpande[1] [Color figure can be viewed at wileyonlinelibrary.com]

measured in an oxygen-deficient electrolyte (purged with nitrogen) to estimate the anodic dissolution of the metal correctly. Microelectrodes with the former polarization curve act as cathodes, while microelectrodes with the latter one become anodes. The polarization curves of zinc and an exemplary distribution of the boundary conditions are shown in Figure 2. After constant time intervals, the boundary conditions of the microelectrodes are randomly distributed to assure macroscopic uniform corrosion progress.

2.3 | Modeling corrosion products

This section aims to give a brief and by no means complete overview over empirical/semiempirical corrosion product models by qualitatively comparing the corrosion progress $y(t)$ and the time-dependent corrosion rate $y'(t)$.[20] The first four models are empirical, that is, the corrosion progress $y(t)$ is proposed and the parameters of the function can be fitted to experimental data.[4,5,7,9] The 5th and 6th model propose a semiempirical modification of the effective corrosion rate in FEM simulations,[10] while a full numerical approach like from Höche[6] or Sun et al.[21] is not considered due to complexity. The corrosion progress of these two semiempirical models is given by the time-integral $y(t) = \int_0^t dt^* y'(t^*)$ and can be used as pure empirical models as well.

a) Ritchie et al.,[4]this simple model assumes a linear corrosion progress, that is, the corrosion rate is constant and does not change over time due to corrosion products.

$$y_{\mathrm{R}}(t) = a \times t. \tag{4}$$

a is the constant corrosion rate. Other authors assume a nonlinear corrosion progress on short timescales and a linear progress on long time scales.[7,16]

b) Yamamoto,[5] he proposes a power law for the corrosion progress

$$y_{\mathrm{Y}}(t) = d \times t^{a}. \tag{5}$$

This publication considers the breakdown of the paint coat as well. This offset is neglected for better comparison. The exponent α lies usually in the range between 0.5 and 1 and empirically describes lowering of the corrosion rate due to limiting processes like diffusion. The factor d describes the length scale of the observed corrosion progress. The growth rate then is

$$y'_{\mathrm{Y}}(t) = ad \times t^{a-1}. \tag{6}$$

c) Soares and Garbatov,[9] these authors assume an asymptotic approach of the corrosion progress towards a steady-state depth d_∞

$$y_{\mathrm{GSG}}(t) = d_\infty(1 - \mathrm{e}^{-t/\tau}). \tag{7}$$

The characteristic time of reaching the steady-state is given by τ. The time-offset due to a coating barrier is here again neglected. The corrosion rate is given by

$$y'_{\mathrm{GSG}}(t) = \frac{1}{\tau}(d_\infty - y_{\mathrm{GSG}}(t)) = \frac{d_\infty}{\tau}\mathrm{e}^{-t/\tau}. \tag{8}$$

A similar expression is also used to model the influence of corrosion products on aluminum via FEM simulations.[22]

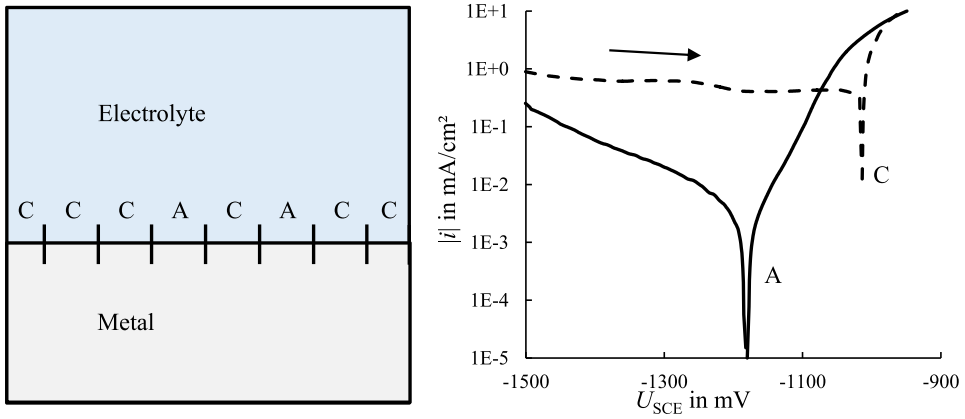

FIGURE 2 Left: Uniform corrosion is modeled via random distribution of anodes (A) and cathodes (C). Right: Polarization curves of zinc in oxygen-deficient (solid line) and oxygen-rich (purged with O_2, dashed) 5 wt.% NaCl electrolyte at 20°C. The arrow indicates the change of polarization[15] [Color figure can be viewed at wileyonlinelibrary.com]

d) Nidadavolu et al. and Dahms et al.,[7,8] the empirical expression of the corrosion progress given by Nidadavolu et al. and Dahms et al. has the following implicit form

$$y_N(t) = y_0(1 - e^{-y_N(t)/y_0}) + \dot{y}_\infty t. \tag{9}$$

y_0 is the corrosion depth on short time scales and $\dot{y}_\infty$ is the long-term corrosion rate. The implicit corrosion rate is given by

$$y'_N(t) = \frac{\dot{y}_\infty}{1 - e^{-y_N(t)/y_0}} \tag{10}$$

where the parameter y_0 describes the initial period which is driven by electrode kinetics and $\dot{y}_\infty$ the steady-state situation which is determined by a limiting process again.

e) Brown et al. and Barnard et al.,[10,23] in this FEM simulation the corrosion rate hindered by corrosion products, for example zinc hydroxide, is given by

$$y'_{BB}(t) = a(1 - p)^2 = a(1 - by_{BB}(t))^2. \tag{11}$$

a is a constant factor and $p(t)$ is the volume fraction occupied by corrosion products between 0 and 1. A constant fraction of the dissolved metal precipitates as corrosion products in this model, in other words $p = by_{BB}$. Time integration of Equation (11) yields

$$y_{BB}(t) = \frac{at}{abt + 1}. \tag{12}$$

This explicit form is not directly used in the model of the original study, but serves for comparison in the present study.

f) New approach

This article proposes another approach to model and implement the effect of corrosion products. These are modeled implicitly, which means an occurring corrosion product layer is not modeled as a separate phase via a mathematical expression. Instead, the average corrosion depth y_{corr} is taken as a measure of the precipitated corrosion products directly. These hinder the diffusion of the reactants, especially the oxygen for the cathodic reaction, and thus lower the effective anodic current density by a factor $c(y_{corr})$

$$i_{eff} = i_a \times c(y_{corr}(t)). \tag{13}$$

y_{corr} is the average corrosion depth at the current time t and is computed as the ratio of the already dissolved metal area and the total length of the metal surface as shown in Figure 3.

This prefactor is proposed to decay exponentially with increasing corrosion depth

$$c(y_{corr}) = \exp\left(-\frac{y_{corr}}{d^*}\right). \tag{14}$$

d^* is a characteristic corrosion depth for a specific combination of metal and electrolyte. In other words, the parameter d^* describes how much dissolved corrosion products precipitate on the surface and how much these hinder the diffusion processes. Thus the corrosion rate is

$$\frac{dy_{corr}(t)}{dt} = \frac{i_{eff}M}{z\rho F} = r\exp\left(-\frac{y_{corr}(t)}{d^*}\right). \tag{15}$$

$r = i_a M/(z\rho F)$ is the corrosion rate without the influence of corrosion products. Assuming $r = \text{const}$, the analytical solution of Equation (15) is

$$y_{corr}(t) = d^* \ln\left(1 + \frac{rt}{d^*}\right). \tag{16}$$

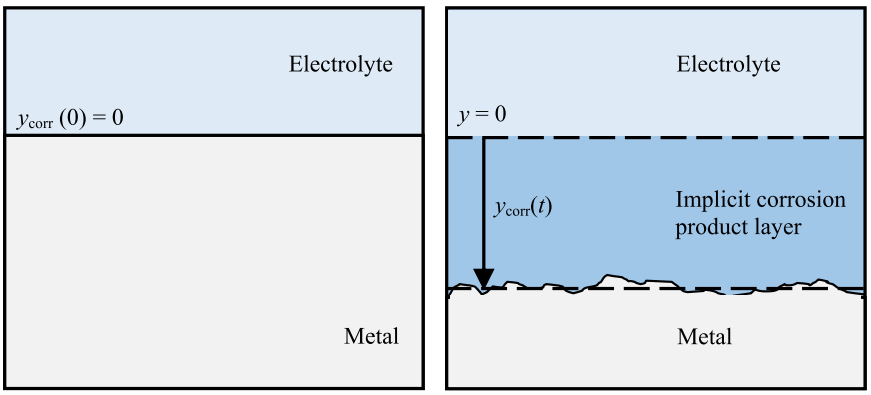

FIGURE 3 Average corrosion depth at time $t = 0$ is $y = 0$ (left) and is increasing with time, $y(t) > 0$ (right) [Color figure can be viewed at wileyonlinelibrary.com]

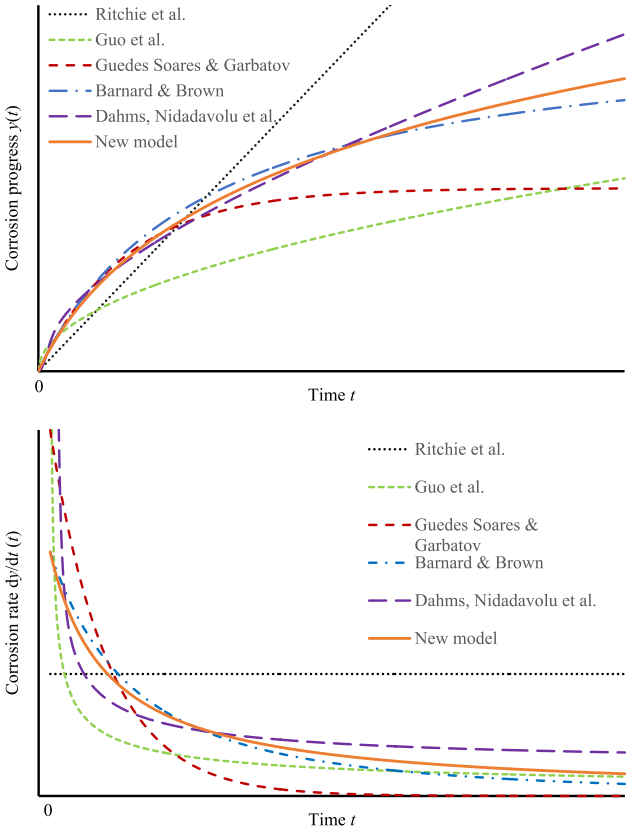

FIGURE 4 Qualitative comparison of corrosion depth (top) and corrosion rate (bottom) over time for various models for corrosion products [Color figure can be viewed at wileyonlinelibrary.com]

Thus, Equation (15) can be rewritten with (16)

$$\frac{\mathrm{d}y_{\mathrm{corr}}(t)}{\mathrm{d}t} = \frac{r}{1 + rt/d^*} = \frac{rd^*}{rt + d^*}. \tag{17}$$

The characteristic time scale for the decrease of the corrosion rate is then given by

$$\tau \sim d^*/r. \tag{18}$$

The limit of Equation (16) for $d^* \to \infty$ yields the constant growth, which can be shown using the inverse $e = 1/d^*$ and L'Hôpital's rule

$$\begin{aligned}\lim_{d^*\to\infty} d^* \ln\left(1 + \frac{rt}{d^*}\right) &= \lim_{e\to 0} \frac{1}{e} \ln(1 + rte) \\ &= \frac{\lim\limits_{e\to 0} \frac{\mathrm{d}}{\mathrm{d}e} \ln(1 + rte)}{\lim\limits_{e\to 0} \frac{\mathrm{d}}{\mathrm{d}e} e} = \frac{\lim\limits_{e\to 0} rt/(1 + rte)}{\lim\limits_{e\to 0} 1} \\ &= rt.\end{aligned} \tag{19}$$

2.4 | Solver aspects

The numerical solutions are computed by the commercial software Comsol Multiphysics® version 5.1 via the FEM. The electrolyte potential ϕ considering the IR-drop due to the finite conductivity (Equations (1) and (2)) is solved by a direct solver called MUMPS.[24] The subsequent displacement of the anodic boundaries in normal direction due to dissolution during time interval Δt (Equation (3)) is explicitly tracked with the arbitrary Lagrangian–Eulerian method.[25] When the distortion of the finite elements or so-called mesh exceeds a threshold, the simulation software computes a new distortion-free mesh. The time integration of the solution is computed with the backward differentiation formula (implicit solver) with order five and the time steps are chosen implicitly as well. In other words, the solver is allowed to take large time steps when there is a high convergence.

3 | RESULTS AND DISCUSSION

3.1 | Comparison of models

The six models from Section 2.3, which take corrosion products into account, are compared in Figure 4. The purpose is the qualitative comparison of the corrosion progress and the corrosion rate. The arbitrarily chosen parameters of these functions are listed in Table 1. Each model, except for the linear model (a) by Ritchie et al., yields a monotonously decreasing corrosion rate over time, which is typical for a limiting process being involved in the corrosion system. The long-term corrosion rate approaches zero except for case (a) by Ritchie et al. and (d) Nidadavolu et al. and Dahms et al. These two models have a finite long-term corrosion rate larger zero, that is, the corrosion progress grows linearly for $t \to \infty$.

At the onset of the corrosion process, the corrosion rate has a finite value for models (a), (c), (e), and (f). Model (b)

TABLE 1 Parameters of corrosion product models used in Figure 4 for qualitative comparison

Model	Ritchie et al.	Yamamoto	Soares and Garbatov	Nidadavolu et al. and Dahms et al.	Brown et al. and Barnard et al.	New approach
Parameter	$a = 0.5\,\mathrm{mm/a}$	$d = 0.7\,\mathrm{mm}$ $a = 0.5$	$d_\infty = 1.5\,\mathrm{mm}$ $\tau = 1.5\mathrm{a}$	$y_0 = 1.5\,\mathrm{mm}$ $\dot{y}_\infty = 0.15\,\mathrm{mm/a}$	$a = 1\,\mathrm{mm/a}$ $b = 0.35\,\mathrm{mm^{-1}}$	$d = 1\,\mathrm{mm}$ $\tau = 1\mathrm{a}$

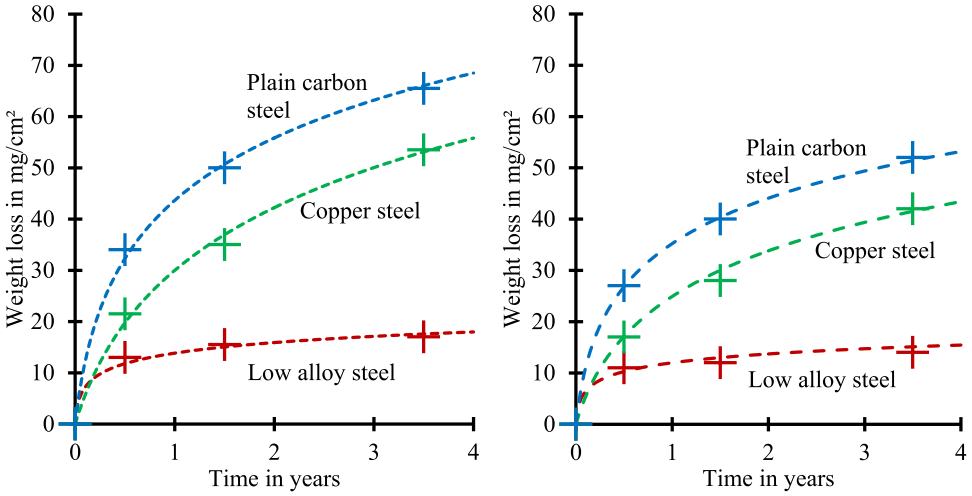

FIGURE 5 Weight loss due to atmospheric corrosion of different steel types (crosses, data from Larabee[26]) and fit with Equation (16) (dashed lines). Steel sheets are tilted 30° to the horizontal. Left: surface groundward, right: upward [Color figure can be viewed at wileyonlinelibrary.com]

by Yamamoto has a pole at $t = 0$ due the exponent $\alpha - 1$ in the power law for $y'_Y(t)$. Since α is smaller than unity in most cases, $y'_Y(t)$ diverges for small times $t \to 0$. Model (d) by Nidadavolu et al. and Dahms et al. has an infinitely large corrosion rate for $t = 0$ due the denominator becoming zero. Thus, a potential implementation of approach (b) or (d) for FEM simulations has to consider the diverging term. The corrosion rate from model (c) might appear to diverge for $t \to 0$ in Figure 4, but is actually finite, $y'_{GSG}(0) = d/\tau_\infty$.

The corrosion progress $y(t)$ is monotonously increasing for all models. However, Soares and Garbatov propose an asymptotic limit for $y_{GSG}(t)$ given by parameter d_∞. Model (e) by Brown et al. and Barnard et al. also yields a maximum corrosion depth given by $y_{BB}^{max} = 1/b$. The corrosion progress of models (a) and (d) increases linearly on long time scales, while the remaining models (b) and (f) continue to grow "slowly."

The here presented logarithmic model (f) behaves similar to the model (e) by Brown et al. and Barnard et al. for short and intermediate time scales and differ for $t \to \infty$ as discussed above. Thus, corrosion systems which do not perfectly passivate can be described more accurate. The advantage of the new model is that the deposit of the corrosion products does not need to be computed explicitly.

3.2 | Application to experimental data

The new approach is applied to various experimental data from corrosion tests of different materials to demonstrate its versatility as an empirical model. The weight loss of various steel types due to atmospheric corrosion is shown in Figure 5.[26] The left diagram shows data of corroding metal sheets facing groundward and the right diagram for upward facing sheets. The slow-down of the corrosion due to corrosion products can be described very well with the new approach for all three steel types and both facing directions. Both parameters of Equation (16) for each fit are listed in Table 2. The initial corrosion rate r of each steel type is assumed to be identical for the

TABLE 2 Parameters of Equation (16) for atmospheric corrosion of various steels from Figure 5

	Surface groundward			Surface upward		
Parameter	**Plain carbon steel**	**Copper steel**	**Low alloy steel**	**Plain carbon steel**	**Copper steel**	**Low alloy steel**
Corrosion rate r (mg/[cm^2·year])	170	64	300	170	64	300
Corrosion product parameter d_* (mg/cm^2)	19	22	3.0	13.5	15	2.5
Corrosion rate r (mm/year)	0.22	0.08	0.38	0.22	0.08	0.38
Corrosion product parameter d_* (μm)	24	28	3.8	17	19	3.2

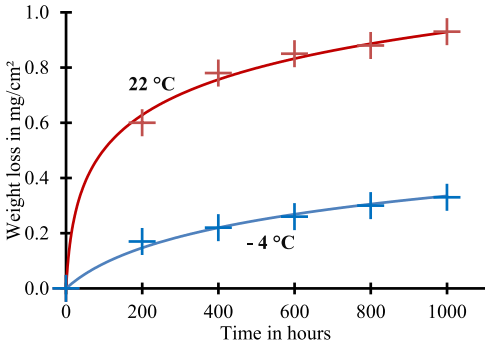

FIGURE 6 Fitting of experimental data[27] for uniform corrosion of zinc with Equation (16) for two different temperatures [Color figure can be viewed at wileyonlinelibrary.com]

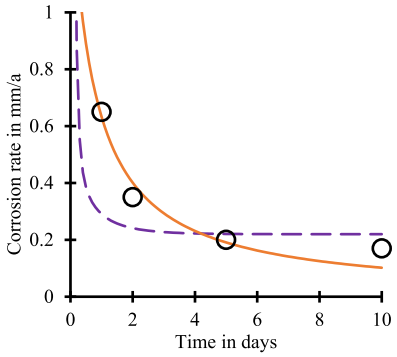

FIGURE 7 Corrosion rate of magnesium alloy Mg-0.3Ca in cell culture medium (circle).[7] Fitting with model by Nidadavolu et al. (dashed line) and new approach (solid line) [Color figure can be viewed at wileyonlinelibrary.com]

groundward and the upward direction since the electrochemical processes should not be influenced by the metal surface direction. However, the groundward face of the metal sheets dries slower due to the lack of sunshine and the electrolyte might drip off from the metal sheets before the corrosion products precipitate.[26] Hence, the weight loss of the groundward metal sheets is about 1.3 higher than for the upward direction. This behavior is described by the corrosion product parameter d^*, which is also about 1.3 higher for the groundward direction.

Figure 6 displays the weight loss of zinc due to atmospheric corrosion for two different temperatures (22°C and − 4°C).[27] The experimental data can be fitted very well by Equation (16). The corresponding parameters are listed in Table 3. The increase of temperature by 26°C significantly raises the initial corrosion rate r by a factor of about 13. This is caused by the change of corrosion product composition, as reported by the experimental work of Esmaily et al.[27] A zinc oxide layer (ZnO) forms on the metal surface for temperatures above − 0.5°C, while the predominant corrosion product is zinc hydroxide ($Zn(OH)_2$) below − 0.5°C. The later one is electrical insulating (dielectric) and leads to a lower corrosion rate. Thus, the corrosion product parameter d^* is about twice as large for 22°C compared to − 4°C.

The corrosion rate of magnesium alloy Mg-0.3Ca in a cell culture medium is shown in Figure 7 to allow long-term prediction when used as implants.[7] The corrosion rate is high during the first days and gradually decreases over the course of 10 days. The authors of the experimental work describe the data with Equation (10) ($\dot{y}_\infty = 0.19\,\text{mm/a}$, $h_0 = 0.22\,\mu\text{m}$). According to the new approach, the corrosion data are approximated with Equation (16) ($r = 1.5\,\text{mm/ a}$,$d^* = 3\,\mu\text{m}$). Thus, a finite initial corrosion rate can be extrapolated for $t = 0$ and the long-term corrosion rate continually decreases.

TABLE 3 Parameters of Equation (16) for atmospheric corrosion of zinc from Figure 6

Parameter	Zinc, 22°C	Zinc, −4°C		Zinc, 22°C	Zinc, −4°C
Corrosion rate r (mg/[cm²·hr])	0.025	0.002	Corrosion rate r (mm/year)	0.31	0.02
Corrosion product parameter d^* (mg/cm²)	0.19	0.11	Corrosion product parameter d^* (μm)	0.27	0.15

3.3 | Simulation of uniform corrosion—zinc case

The new approach can be easily implemented into FEM simulations especially if they are based on the MPT. The corrosion progress of a zinc sheet in 5% NaCl solution is simulated using the polarization curves of Figure 2 as boundary conditions as described in Section 2.2 with $d^* = 1\,\mu\text{m}$. The deformed geometry for various

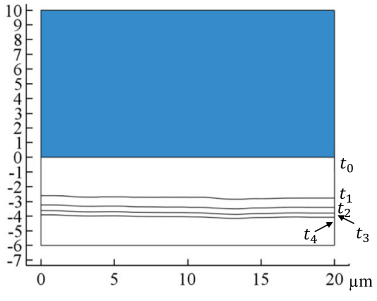

FIGURE 8 Deformed macroscopic geometry due to uniform corrosion of zinc in 5 wt.% NaCl for $t_0 = 0\,\text{s}$, $t_1 = 7 \times 10^5\,\text{s}$, $t_2 = 1.4 \times 10^6\,\text{s}$, $t_3 = 2.1 \times 10^6\,\text{s}$, and $t_4 = 2.8 \times 10^6\,\text{s}$ [Color figure can be viewed at wileyonlinelibrary.com]

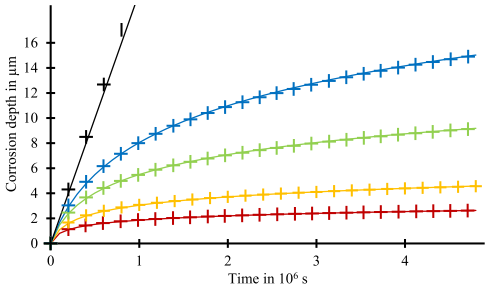

FIGURE 9 Comparison of FEM results (crosses) and analytical expression (solid lines, Equation (16)) for four different parameters d^*: 0.5 µm (red), 1.0 µm (orange), 2.5 µm (green), and 5.0 µm (blue). Black represents the results without influence of corrosion products [Color figure can be viewed at wileyonlinelibrary.com]

equidistant time steps is shown in Figure 8. While the corrosion progress is large after the first time interval ($y_{corr} \cong 2\,\mu m$), the progress in the second time interval is already less than 1 µm and decreases further with increasing time. The characteristic time scale for the decrease of the corrosion rate according to Equation (18) is $\tau \sim d^*/r = 1\,\mu m/(1.95 \times 10^{-5}\,\mu m/s) \sim 5 \times 10^4\,s$ (around 14 hr).

The non-linear influence of the corrosion product parameter d^* is demonstrated in Figure 9. The analytical corrosion progress from Equation (16) is compared to the FEM results for following values of d^*: 0.5 µm, 1.0 µm, 2.5 µm and 5.0 µm. Increasing the parameter d^* decreases the influence of the corrosion products in the simulations. Choosing an arbitrarily large value for $d^* \gg 1$ yields the linear behavior, as shown in Equation (19). The FEM results agree very well with the analytic expression, which demonstrates the robustness of the implementation. Even more, it proves its applicability to a wide range of corrosion phenomena and materials with changing driving mechanisms during corrosion progress.

4 | CONCLUSIONS

This work presents a new implicit description of corrosion product implementation into predictive corrosion models, which can be used for numerical simulations or empirical predictions of uniform corrosion progress as well. This new approach assumes that dissolved metal precipitates or converts on the metal surface in a corrosion product and reduces the initial corrosion rate r due to insulating properties and reduction of the active species transport (e.g., lower effective diffusion coefficient). The strength of this effect is governed by the so-called corrosion product parameter d^*, which also belongs to a characteristic corrosion depth of the investigated system. Thus, this variable combines the physical and chemical properties in a single parameter enabling long-term predictions of uniform corrosion (excluding a change in the mechanism). Assuming a constant initial corrosion rate r, the corrosion progress is given by $d^* \ln(1 + (rt/d^*))$. The effective corrosion rate is finite for $t = 0$ and asymptotically approaches zero for $t \to \infty$.

This approach is compared with other empirical descriptions of corrosion progress accounting for corrosion products and explicit corrosion product models for FEM based simulations. Since the former models propose either an infinitely large initial corrosion rate or linear growth for $t \to \infty$ and the explicit (numerical) models require the computation of the diffusion, migration and formation of all participating chemical species, these approaches are not suitable for fast and accurate prediction. The validity of the current approach is demonstrated with experimental data for various materials, where the measured corrosion progress can be very well described with the proposed analytical equation. This implicit model can be seamlessly implemented in any numerical simulations, as shown for the uniform corrosion of zinc. In addition, it might be useful as an empirical model with two physical parameters. Thus, this model is able to make predictions about the further corrosion progress when experimental data are given and to physically interpret these parameters, that is, the initial corrosion rate and the corrosion product parameter.

ACKNOWLEDGMENTS

Tom Gießgen wishes to acknowledge Julia Rößler and Hermann Müller for their laboratory support.

ORCID

Tom Gießgen http://orcid.org/0000-0002-2325-0163
Daniel Höche http://orcid.org/0000-0002-7719-6684
Mikhail Zheludkevich http://orcid.org/0000-0002-9658-9619
Karl U. Kainer http://orcid.org/0000-0002-9630-0985

REFERENCES

[1] K. B. Deshpande, *Corros. Sci.* **2010**, *52*, 3514.
[2] K. B. Deshpande, *Electrochim. Acta* **2011**, *56*, 1737.
[3] N. C. Bösch, D. Höche, A. Mittelbach, K. U. Kainer, *Mater. Corros.* **2017**, *68*, 699.
[4] D. Ritchie, C. W. M. Voermans, M. H. Larsen, W. R. Vranckx, 17th Int. Conf. Offshore Mechanics and Arctic Engineering, Lisbon, Portugal, July, 1998, p. 5.
[5] N. Yamamoto, *Nippon Kaiji Kyōkai NK Tech. Bull.* **1997**, 43.

[6] D. Höche, *J. Electrochem. Soc.* **2015**, *162*, C1.
[7] E. P. S. Nidadavolu, F. Feyerabend, T. Ebel, R. Willumeit-Römer, M. Dahms, *Materials* **2016**, *9*, 627.
[8] M. Dahms, D. Höche, N. Ahmad Agha, F. Feyerabend, R. Willumeit-Römer, *Mater. Corros.* **2017**, *13*, 156.
[9] C. G. Soares, Y. Garbatov, *Mar. Struct.* **1999**, *12*, 425.
[10] N. C. Barnard, S. G. R. Brown, H. N. McMurray, in *Simulation of Electrochemical Processes* (Eds: C. A. Brebbia, V. G. DeGiorgi, R. A. Adey), WIT Press, Southampton, UK **2005**, p. 99.
[11] Y. Wang, L. Yin, Y. Jin, J. Pan, C. Leygraf, *J. Electrochem. Soc.* **2017**, *164*, C1035.
[12] D. Snihirova, D. Höche, S. Lamaka, Z. Mir, T. Hack, M. L. Zheludkevich, *Corros. Sci.* **2019**, *157*, 70–78
[13] Z. M. Mir, D. Höche, C. Gomes, R. Sampaio, A. C. Bastos, P. Maincon, M. G. S. Ferreira, M. L. Zheludkevich, *Int. J. Concr. Struct. Mater.* **2019**, *13*, 1047.
[14] N. C. Bösch, *PhD Thesis*, TU Hamburg-Harburg, (Hamburg-Harburg) 2017.
[15] T. Gießgen, A. Mittelbach, D. Höche, M. Zheludkevich, K. U. Kainer, *Mater. Corros.* **2018**, *69*, 1720.
[16] R. E. Melchers, *Struct. Infrastruct. Eng.* **2018**, *14*, 843.
[17] L. A. Shaik, S. K. Thamida, *J. Electroanal. Chem.* **2016**, *780*, 264.
[18] D. R. Lide, *CRC Handbook of Chemistry and Physics*, Chemical Rubber Publishung Company, Boca Raton, FL **2004**.
[19] M. Faraday, *Philos. T. R. Soc. Lond.* **1834**, *124*, 77.
[20] D. Höche, E. Gazenbiller, B. Daneshian, T. Gießgen, A. Mittelbach, N. Konchakova, L. Sviatlana, C. Feiler, Z. Mir, D. Snihirova, T. Würger, R. H. Meißner, M. L. Zheludkevich, K. U. Kainer, in *3-Länder-Korrosionstagung*, Frankfurt/Main, Germany **2019**.
[21] W. Sun, L. Wang, T. Wu, G. Liu, *Corros. Sci.* **2014**, *78*, 233.
[22] L. Yin, Y. Jin, C. Leygraf, J. Pan, *Electrochim. Acta* **2016**, *192*, 310.
[23] S. G. R. Brown, N. C. Barnard, in *Simulation of Electrochemical Processes II* (Eds: V. G. DeGiorgi, C. A. Brebbia, R. A. Adey), WIT Press, Myrtle Beach, SC **2007**, p. 3.
[24] P. R. Amestoy, I. S. Duff, J. Y. L'Excellent, *Comp. Meth. Appl. Mech. Eng.* **2000**, *184*, 501.
[25] J. Donea, A. Huerta, J. P. Ponthot, A. Rodríguez-Ferran, in *Encyclopedia of Computational Mechanics* (Eds: E. Stein, T. J. R. Hughes, R. de Borst), Wiley, New York, NY **2004**.
[26] C. P. Larrabee, *Trans. Electrochem. Soc.* **1944**, *85*, 297.
[27] M. Esmaily, N. Mortazavi, J. E. Svensson, L. G. Johansson, *J. Electrochem. Soc.* **2016**, *163*, C864.